iScience

CellPress
OPEN ACCESS

Article

Maximizing electrical power through the synergistic utilization of solar and space energy sources

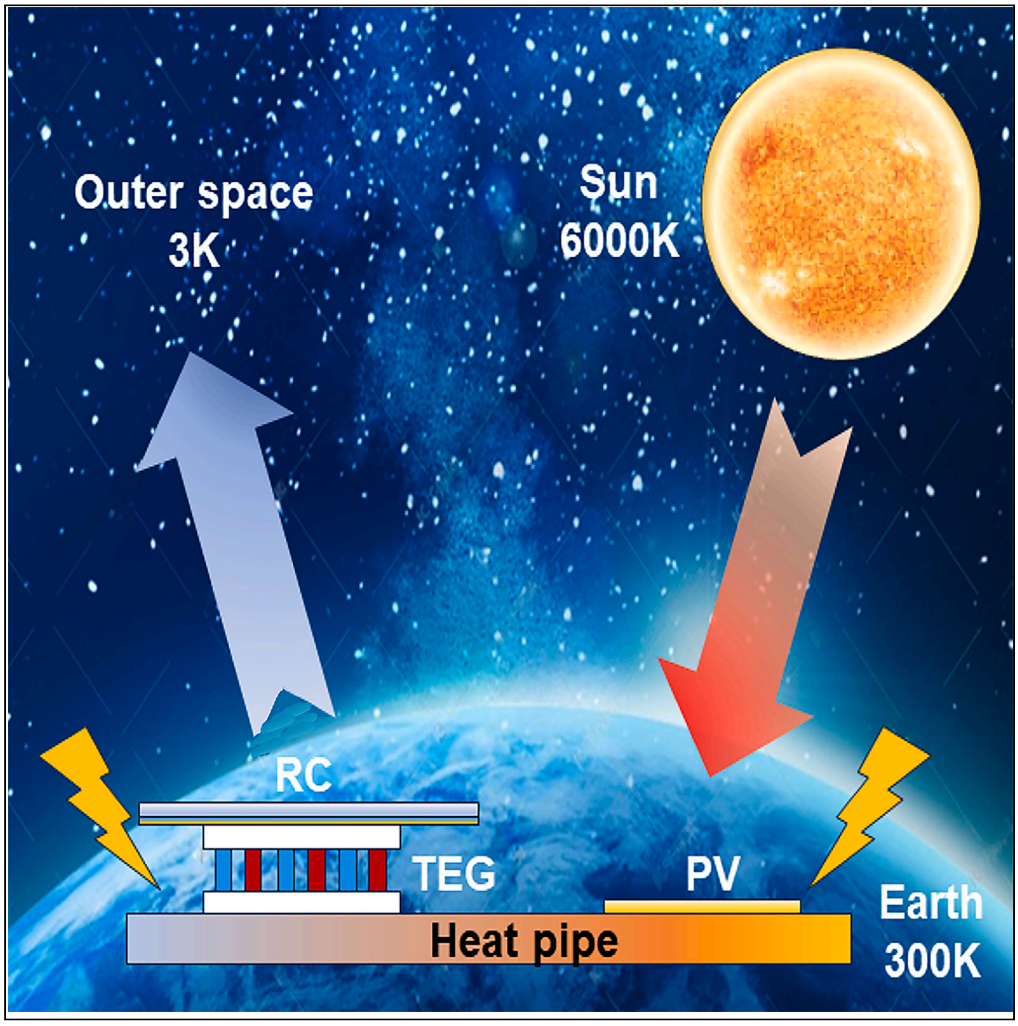

Song Lv, Haoliang Bai, Juwen Ren, ..., Shangzhen Xie, Yirong Deng, Yishuang Ji

lvsong@whut.edu.cn (S.L.)
ysji@whut.edu.cn (Y.J.)

Highlights

The first instances of adding a photovoltaic to the RC-TE system

Generate electricity by synergistically harnessing two thermodynamic resources

Enables PV thermal management and boosts thermoelectric power generation

3D transient coupled simulation models accurately predict operating limits

Lv et al., iScience 27, 109952
June 21, 2024
https://doi.org/10.1016/j.isci.2024.109952

iScience

CellPress
OPEN ACCESS

Article

Maximizing electrical power through the synergistic utilization of solar and space energy sources

Song Lv,[1,2,5,*] Haoliang Bai,[1] Juwen Ren,[1] Bolong Zhang,[1] Yin Lai,[1] Jiahao Yang,[1] Zhihao Chang,[1] Shangzhen Xie,[3] Yirong Deng,[4] and Yishuang Ji[1,*]

SUMMARY

The sun and outer space are two crucial renewable thermodynamic resources that work together to maintain the delicate energy balance of our planet. The challenge lies in harvesting both resources synergistically and converting them into high-quality electricity. Here, we introduce a photovoltaic thermoelectric radiative cooling (PV-TE-RC) system. This system uses the full spectrum of the sun and the atmospheric window to generate electricity and achieve high-quality collaborative utilization of solar energy and space energy. Outdoor experiments have demonstrated the system's capacity to operate efficiently around the clock. Notably, during the peak solar concentration, the thermoelectric generator (TEG) and the system achieved power outputs of 870 mW/m^2 and 85.87 W/m^2, respectively. We have further developed a three-dimensional transient coupled simulation model, which can accurately predict its operational limits. Therefore, this study provides practical insights and recommendations for large-scale and efficient collaborative power generation using these two thermodynamic resources.

INTRODUCTION

The world is facing increasingly severe energy crises and climate challenges, heightening the importance of developing renewable energy as a substitute for fossil fuels.[1] Solar energy and outer space represent the two most critical renewable thermodynamic resources, yet the majority of research has focused solely on harnessing one of these resources. Concerning the collection of space energy, radiative cooling (RC) technology plays a pivotal role by releasing heat radiation into space. The performance of the radiative cooler continues to improve due to advancements in material engineering,[2–9] although its cooling power remains constrained by the surface area.[10] The collection of solar energy is primarily accomplished through photovoltaic or photothermal conversion. Photovoltaic (PV) cells can directly convert sunlight into electricity. However, the efficiency of traditional single-junction PV cells is restricted to 33% due to a substantial portion of the solar spectrum that cannot be utilized for photovoltaic conversion.[11] With advancements in new materials and structural engineering, solar energy absorbers can achieve almost 100% absorptivity under AM1.5G (1 kW/m^2) conditions.[12–14] Yet, converting it into higher-grade electricity requires leveraging the thermoelectric conversion effect, with the overall efficiency constrained by thermoelectric (TE) materials and temperature gradients.[15–18] Previous research has revealed that the theoretical limits of harnessing energy from both thermodynamic resources far exceed those of relying on a single energy source, thus overcoming the limitations of solitary energy collection.[19,20] Consequently, the synergistic utilization of solar and cosmic energy is gradually emerging as a key research focus.

Since the breakthrough of daytime radiative cooling technology in 2014,[21] researchers have embarked on exploring the collaborative utilization of solar energy and space cold sources in the form of heat energy.[22,23] Compared to heat, electricity is a higher quality energy source. Nevertheless, the conversion of these two thermodynamic resources into more advanced electricity remains a challenge. With the development and integration of thermoelectric technology and RC technology, the utilization of solar energy and space cold source energy for power generation has become a possibility. Researchers have proposed radiative cooling-driven thermoelectric power generation (RC-TE) systems, which have been proven to be effective.

Presently, research on RC-TE power generation systems primarily centers on materials and design aspects. Concerning materials, researchers are dedicated to developing novel RC materials with high emissivity in the atmospheric window and low absorption of the solar spectrum. This involves the incorporation of various strategies, including the utilization of porous structures,[24] nanomaterials,[25–27] and infrared radiation materials,[28–31] aimed at maximizing the absorption of energy from the cosmic cold source. Additionally, the optimization

[1]School of Naval Architecture, Ocean and Energy Power Engineering, Wuhan University of Technology, Wuhan 430063, China
[2]School of Materials Science and Engineering, Wuhan University of Technology, Wuhan 430063, China
[3]School of Energy and Environment, City University of Hong Kong, Tat Chee Avenue, Kowloon Tong, Hong Kong, China
[4]Faculty of Engineering, The University of Hong Kong, Pokfulam, Hong Kong, China
[5]Lead contact
*Correspondence: lvsong@whut.edu.cn (S.L.), ysji@whut.edu.cn (Y.J.)
https://doi.org/10.1016/j.isci.2024.109952

of heat transfer materials is considered a key means to enhance power generation efficiency, as efficient heat transfer materials can reduce the heat exchange between the system and the surrounding environment, thus minimizing thermal losses and enhancing energy utilization efficiency.[32] Studies focusing on optimizing the design primarily explore spiral structures[33] and biomimetic structures.[34] Moreover, some have proposed the integration of the TEG's hot side with human body heat sources.[25–27,31] Therefore, it is possible to flexibly adjust system parameters and manage heat flow direction based on the specific system structure and application context.

Nevertheless, even though some RC-TE systems have achieved electricity generation from solar energy and space cold source energy, achieving high power generation efficiency remains challenging due to the constraints imposed by thermoelectric materials and the temperature difference between the hot and cold sides. Currently, the highest value stands at only 185.9 mW/m^2,[27] which can supply tiny mW and μW sensors or LEDs, making large-scale practical applications infeasible. While photovoltaic cells exhibit higher power density, their average cost remains relatively high due to the limitations imposed by the day-night cycle. To achieve full-spectrum utilization and energy cascade utilization, the integration of a novel energy conversion mechanism combining photovoltaic, photothermal, thermoelectric, and radiative cooling has become feasible.[35] However, without energy storage, the actual electricity generation capacity of the system during the day and night remains a challenge.

This study introduces, for the first time, a PV-TE-RC power generation system that integrates photovoltaic, thermoelectric, and radiative cooling technologies. This system transcends the fundamental constraints associated with harvesting energy from the sun and space, surpassing the efficiency of any existing collaborative power generation scheme that harnesses both thermodynamic resources. Experimentally, we employed a cascaded connection between the radiative cooling module and the thermoelectric module, while the thermoelectric module and the photovoltaic cell module are indirectly linked via heat pipes, enabling a continuous collection of energy from the sun and outer space through the concerted operation of the three modules. We demonstrated that the thermoelectric generator (TEG) achieves an average power of 870 mW/m^2 under one day's peak sunlight in Wuhan, China in late October, which is 4.6 times higher than the electrical power output of RC-TE systems in recent studies.[27] Moreover, the system's total output reached 85.87 W/m^2, achieving efficient and high-quality synergistic utilization of two thermodynamic resources. Moreover, we established, for the first time, a physical model of the PV-TE-RC system to simulate its thermal and electrical behaviors. Leveraging the model, we predicted the system's limitations, showcasing its potential as an independent power source for outdoor, military, and aerospace applications.

RESULTS

PV-TE-RC system

Currently, the coordinated utilization of solar energy and space energy primarily hinges on RC-TE technology. To maximize the collection of solar energy, a solar absorber with high broadband light absorption within the solar spectrum range is employed, while a radiative emitter with minimal sunlight absorption and near-saturated emissivity within the atmospheric transparency window is used to maximize the collection of outer space energy (Figure 1A). However, the RC-TE system encounters constraints arising from thermoelectric materials and the temperature differential between the hot and cold sides, which pose challenges in achieving higher power generation efficiency. Photovoltaic cells offer a direct conversion of solar energy into electricity, showcasing advantages in energy conversion. Nonetheless, photons with energy lower than the bandgap (E_g) cannot be effectively utilized by PV cells and are instead converted into heat energy. Similarly, excess energy from photons with energy greater than E_g, which cannot be harnessed by PV cells, is inevitably transformed into heat energy, as illustrated in Figure 1B. Due to the temperature sensitivity of PV performance, previous literature has primarily dissipated this heat through active or passive radiators,[36–38] leading to additional parasitic energy consumption and device redundancy. Harvesting of this thermochemical energy becomes crucial to improve the system's power generation efficiency. Therefore, the integration of PV and TE-RC technology holds the potential to address the challenges faced by both.

We have introduced an innovative combination of photovoltaic modules, thermoelectric modules, and radiative cooling modules to create a PV-TE-RC system (Figure 1C). In this system, the PV cells and the hot side of the TE module capture solar energy, while the RC film captures energy from outer space and transports it to the cold side of the TE module. By leveraging the temperature difference between the hot and cold sides, the TE module generates electricity, enhancing the overall electrical power output of the system. The physical structure of the PV-TE-RC system is depicted in Figure 1D, with both the photovoltaic cell module and the radiative cooling module oriented toward the sky. The radiative cooling module and the thermoelectric module are interconnected in a cascaded arrangement, with heat pipes indirectly linking the thermoelectric module and the photovoltaic cell module. Thermal conductive silicone grease is used for adhesion between these components. The operational principle of the system is as follows: during daylight hours, the photovoltaic cells absorb solar radiation, producing both electrical energy and some heat, which is conducted at the evaporating side of the heat pipe. Within the heat pipe, the heat transfers to the condensing side through the phase change of the internal heat transfer fluid. The condensing side is connected to the hot side of the TEG, supplying heat to the TEG. The lower section of the radiative cooling module is linked to the cold side of the TEG, releasing heat into the cold outer space through the atmospheric window (8–13 μm) to provide cooling for the TEG. When a temperature differential exists between the two sides of the TEG, the Seebeck effect induces the carriers at the hot side to diffuse toward the cold side, accumulating charges and generating an electric field within the conductor. This electric field opposes the carriers, impeding their further diffusion, ultimately reaching a dynamic equilibrium and producing electrical energy. The waste heat from the photovoltaic cell module passes through the thermoelectric module and dissipates from the top of the radiative cooling module, thereby reducing the cell's temperature and enhancing its electrical output. During the night, the TEG's cold side leverages radiative cooling to draw in the chill from outer space, effectively lowering its temperature. This temperature disparity between the cold side and the ambient temperature on the hot side is converted into electrical energy

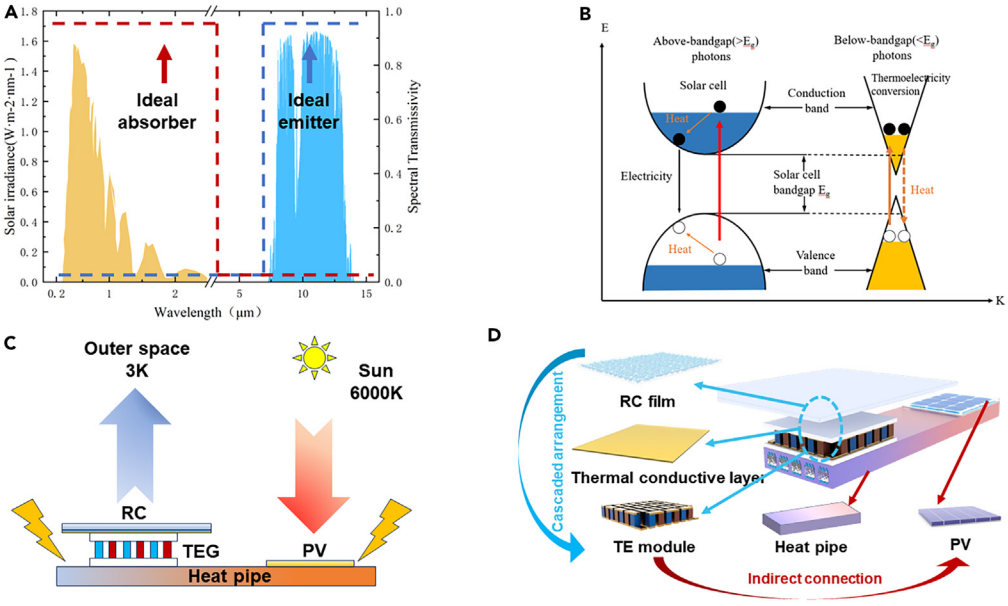

Figure 1. PV-TE-RC system using solar energy and space energy synergistically converted into electricity

(A) Ideal absorption spectrum of solar energy and ideal spectrum of infrared radiation for PV-TE-RC systems.

(B) Band diagram of PV-TE-RC system.

(C) The concept of PV-TE-RC systems for harvesting energy from the sun and cold space.

(D) Internal structure and installation process of the PV-TE-RC system. The details of Modules, test platform and experimental device are mentioned in Figure S1.

via the Seebeck effect. Consequently, the PV-TE-RC system effectively harnesses solar energy and outer space energy for electricity generation from daytime to nighttime, demonstrating commendable energy utilization efficiency and environmental sustainability.

Experimental performance

To demonstrate the full-day power generation potential of the PV-TE-RC system, we conducted performance testing on a rooftop in Wuhan, China, in late October 2022, under clear sky conditions. The testing details can be found in Figure S1.

The symbols involved in this paper are described in Table S4. Figure 2A illustrates the temperature variation trends at five measurement points, namely the device cavity, the back of the photovoltaic cell, the cold side of the TEG, the hot side of the TEG, and the back of the radiative cooling film, during a continuous 24-h measurement period, all exhibiting peaks during daylight sun exposure periods. As the solar irradiance intensity increases, the temperature differentials between the five points gradually enlarge. The results indicate that the system demonstrates favorable radiative cooling performance during the night, with their temperatures being 4°C, 4.9°C, 5.5°C, 6.1°C, and 6.3°C lower than the ambient temperature, respectively. During the concentrated solar irradiation period from 11:00 to 13:00, the maximum temperature differentials between them and the ambient temperature are 18°C, 11.8°C, 10.8°C, 8.3°C, and 7°C, respectively, and the temperature differentials increase with the intensification of irradiance.

The variation trend of the net cooling power in the radiative cooling module over time is depicted in Figure 2B. The cooling power of the radiative cooling module reaches its maximum value during the night, at approximately 78 W/m^2. With the emergence of solar irradiance and its continuous increase in intensity, the radiative cooling power gradually diminishes. When the solar irradiance exceeds 600 W/m^2, the net radiative cooling power becomes negative. This indicates that under such circumstances, the solar radiation provided by the radiative cooling module surpasses the cooling capacity generated by the radiative cooling module itself, rendering the system incapable of providing radiative cooling.

Figure 2C depicts the variations in the output power and conversion efficiency of the photovoltaic cells over time. During the day, the output power of the photovoltaic cells exhibits a positive correlation with the intensity of solar irradiance. The maximum output power is achieved at the peak of solar irradiance, reaching 85 W/m^2, with an average photovoltaic conversion efficiency of 10%. As a result of the cooling effect of the heat pipe, the photovoltaic cells generated 8.97% more power than the independent PV power provided by the manufacturer. Additionally, it can be observed that there is a negative correlation between the photovoltaic conversion efficiency and the irradiance intensity. When the irradiance intensity is at its maximum, the photovoltaic conversion efficiency is relatively lower, at 9.25%. This is because only the photons within the bandgap range are absorbed and converted into electrical energy by the photovoltaic cells, while the remaining photons that are absorbed generate waste heat, leading to an increase in the temperature of the photovoltaic cells. As the irradiance intensity increases, more photons are used for generating heat in the cell, thereby reducing the photovoltaic conversion efficiency. Hence, the photovoltaic conversion efficiency demonstrates a trend of initially decreasing and then increasing.

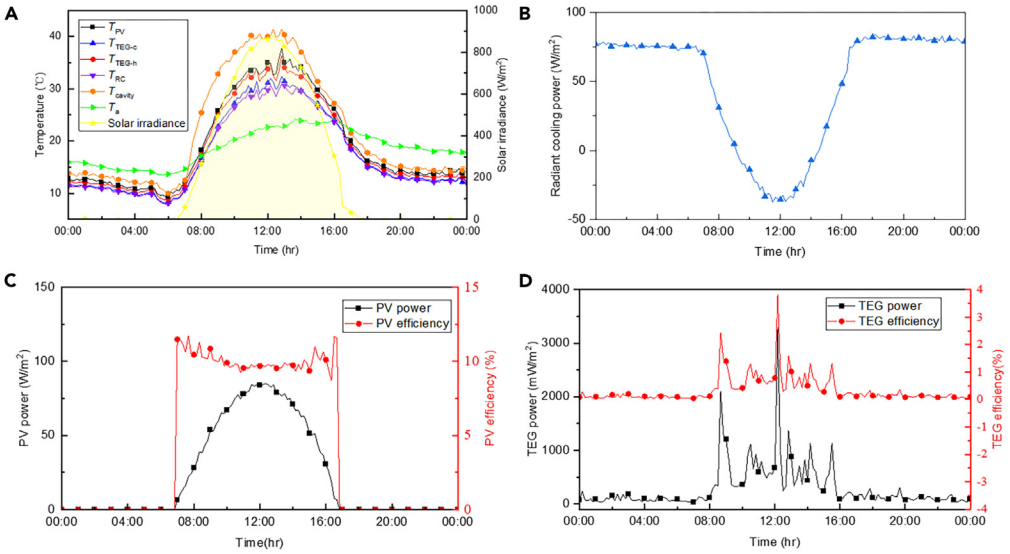

Figure 2. Performance of the PV-TE-RC system in outdoor experiments

(A) Temperatures at each measurement point: back of the PV cell, cold side of the TEG, hot side of the TEG, and back of the radiation-cooled film.

(B) Net radiative cooling power.

(C) Output power and photovoltaic conversion efficiency of PV cell.

(D) Output power and thermoelectric conversion efficiency of TEG.

The variations in the output power and thermoelectric conversion efficiency of the TEG module over time are illustrated in Figure 2D. During the day, the excess heat generated by the solar radiation absorbed by the photovoltaic cells provides a heat flow to the hot side of the TEG. The cold side of the TEG relies on the cooling provided by the radiative cooling membrane for heat dissipation, which increases the temperature difference between the hot and cold sides of the TEG. The TEG's performance is optimized during the concentrated solar irradiance period from 11:00 to 13:00. At this time, the average temperature difference between the hot and cold sides of the TEG is 2.5°C, resulting in an average power generation of 870 mW/m^2 and an average thermoelectric conversion efficiency of 1.01%. This is a 24.29% improvement in power generation compared to the independent RC-TE in our previous study.[39] As the solar irradiance intensity increases, the temperature difference between the hot and cold sides of the TEG also increases, leading to improvements in the output power and thermoelectric conversion efficiency. At night, the average temperature difference between the hot and cold sides of the TEG is 0.6°C, resulting in an average power generation of 96 mW/m^2 and an average thermoelectric conversion efficiency of 0.11%.

The experimental data highlight the significance of solar irradiance intensity and ambient temperature as crucial factors influencing the system's operation. Therefore, conducting a more comprehensive study of environmental factors is essential, as it can contribute to the optimization of the system's design and the enhancement of its performance.

Model validation

The development of a three-dimensional transient coupled simulation model serves as a valuable tool for gaining a deeper understanding of the operational principles of the PV-TE-RC system and for assessing its stability and safety. With the construction of a coupled model for the PV-TE-RC system, it becomes possible to accurately predict its performance under various operating conditions. This includes the photovoltaic power generation performance, thermoelectric conversion performance, and radiative cooling performance. Such a modeling approach also facilitates the optimization of the system's structure and parameters, ultimately leading to improvements in overall system performance. The physical model of the PV-TE-RC system is depicted in Figure 3A, and the model meshing and irrelevance verification is shown in Figure S2. The relevant parameters and materials properties in the physical model are shown in Tables S1 and S2. The specific mesh dimensions are shown in Table S3.

To verify the accuracy of the mathematical model, the present model is calculated according to the relevant parameters of the experimental prototype. A comparison between experimental results and simulation has been performed. The root-mean-square deviation (RMSD)[40] is employed to examine the fitting degree between experimental data and simulation results.

$$RMSD = \sqrt{\frac{\sum \left[\left(X_{sim,i} - X_{exp,i}\right)/X_{exp,i}\right]^2}{n}}$$

where $X_{sin,i}$ and $X_{exp,i}$ are the simulated and experimental values, respectively. n refers to the number of experimental data.

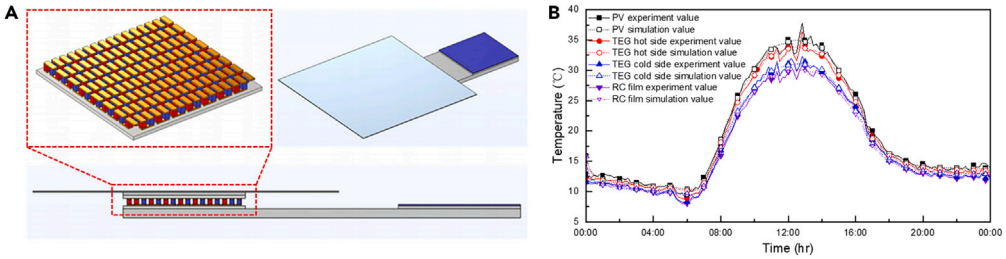

Figure 3. Three-dimensional transient coupled simulation model of PV-TE-RC system

(A) Physical modeling and (B) model validation of the PV-TE-RC system. The details of model meshing and simulated temperatures at different grid sizes are mentioned in Figure S2. The relevant parameters and materials properties in the physical model are shown in Table S1 and S2. The specific mesh dimensions are shown in Table S3.

Figure 3B displays a comparison between the simulated temperatures and the experimental temperatures of various components, including the photovoltaic cell, TEG cold side, TEG hot side, and the bottom of the radiative cooling film. The trends of the experimental temperatures and the simulated temperatures for each component are generally consistent, demonstrating a high degree of agreement. Initially, the simulated temperature values are slightly higher than the experimental temperature values, which can be attributed to the initial values set in the simulation model to match the ambient temperature. However, with time, the simulated temperature values progressively approach and closely align with the actual temperature values, exhibiting minimal error. The maximum temperature differences between the simulated and experimental temperatures for the photovoltaic cell, TEG cold side, TEG hot side, and the bottom of the radiative cooling film all fall within 2°C. Specifically, at 11:40, the maximum temperature disparities between the simulated and experimental values for the four measurement points are 1.56°C, 1.71°C, 1.4°C, and 1.67°C, corresponding to RMSD values of 4.2%, 5.2%, 4.8%, and 2.6%, respectively.

These results affirm that the proposed simulation model for the PV-TE-RC system in this study exhibits high accuracy and can effectively simulate energy conversion in the experimental prototype.

Prediction

To delve deeper into the impact of various environmental parameters on the system's performance, we utilized experimental data from 12:00 as input parameters for the simulation model. We conducted a sensitivity analysis for a range of environmental parameters and different operating parameters of the modules. This comprehensive analysis aims to better understand the mechanisms through which these parameters influence the thermal and electrical performance of the system, ultimately leading to improved system design and enhanced overall performance.

Environmental parameters

Wind velocity

Figure 4A illustrates the influence of wind speed on the temperatures at various points within the PV-TE-RC system. The figure reveals that as the wind speed increases, the temperatures of all system components gradually decrease, accompanied by a reduction in the slope, resulting in a more gradual temperature change. As the wind speed increases from 0 m/s to 10 m/s, the temperatures of the PV module, TEG hot side, TEG cold side, and the radiative cooling film decrease by 8.41°C, 7.78°C, 6.25°C, and 5.69°C, respectively. This phenomenon can be attributed to the presence of a transparent cover on the radiative cooling module, which mitigates the impact of wind speed. The PV module is more significantly affected by wind speed, as an increase in wind speed enhances the convective heat transfer coefficient between the PV module and its surroundings, thereby improving its heat dissipation capacity. Consequently, the heat transferred from the PV module to the TEG module and the radiative cooling module decreases, leading to a temperature decrease at the four measurement points. However, it's worth noting that as the temperature of the PV module approaches that of the surroundings, the impact of further increasing the wind speed on the heat transfer capacity between the PV module and its surroundings becomes limited.

Figures 4B and 4C, respectively, illustrate the influence of wind speed on the output power and efficiency of the PV-TE-RC system. The wind speed is directly proportional to the output power and the photoelectric conversion efficiency of the PV module. As the wind speed increases, the output power and photoelectric conversion efficiency of the PV module also increase, and the increasing trend of these two parameters gradually diminishes as the wind speed continues to increase. As the wind speed increases from 0 m/s to 10 m/s, the PV module's power output increases from 84.39 W/m^2 to 87.55 W/m^2, and the photoelectric conversion efficiency increases from 9.59% to 9.97%. This increase is attributed to the enhancement of the convective heat transfer coefficient between the PV module and its surroundings, leading to improved heat dissipation capacity and consequently reducing the temperature of the PV module, thereby increasing the photoelectric conversion efficiency and output power. However, when the heat transfer coefficient reaches a certain value, further increasing the wind speed has a minimal impact on the temperature of the PV module, resulting in a stable trend in the output power. Wind speed negatively affects the TEG power output, thermoelectric conversion efficiency, and cooling power. As the wind speed increases, all three gradually decrease and tend to stabilize. When the wind speed increases from 0 m/s to 10 m/s, the TEG power output decreases from 0.55 W/m^2 to 0.15 W/m^2, the

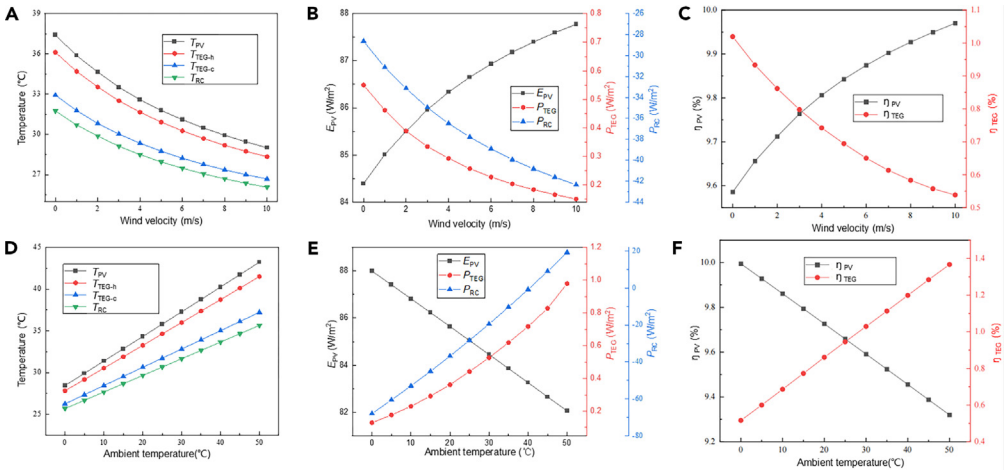

Figure 4. Effect of wind velocity (A–C) and ambient temperature (D–F) on the thermal performance, output power, and conversion efficiency of the PV-TE-RC system

thermoelectric conversion efficiency decreases from 1.02% to 0.539%, and the cooling power decreases from −28.62 W/m^2 to −42.36 W/m^2. Due to the installation of wind shields and insulation layers, the radiation cooling module and the TEG module do not directly contact the external environment. As the wind speed increases, the heat dissipation capacity of the PV module increases, leading to a reduction in the heat flux density it provides to the TEG module and the radiation cooling module, resulting in a decrease in the temperatures of the TEG hot and cold sides as well as the radiation cooling power. The reduction in the cooling power of the radiation cooling module leads to a decrease in the heat flux density at the TEG cold side. Therefore, both the cold and hot-side heat flux densities of the TEG decrease, resulting in a decrease in its power output and thermoelectric conversion efficiency. These results demonstrate that an appropriate range of wind speeds can enable the system to exhibit higher performance.

Ambient temperature

Figure 4D illustrates the impact of ambient temperature on the temperatures of various points within the PV-TE-RC system. It is evident that with an increase in ambient temperature, the temperatures of all measured points rise to varying degrees. Among these, the most significant temperature change is observed for the PV module, which is in direct contact with the environment. Following the PV module, the hot side and cold side of the TEG, and the radiative cooling film exhibit temperature changes. When the ambient temperature increases from 0°C to 50°C, the temperatures of the PV module, TEG hot side, TEG cold side, and radiative cooling film increase by 14.78°C, 13.68°C, 10.97°C, and 9.97°C, respectively. This temperature increase can be attributed to the fact that when the ambient temperature is lower than the temperature of the system components, an increase in ambient temperature leads to a reduction in the temperature gradient between the components and the environment, resulting in decreased heat dissipation. Conversely, when the ambient temperature is higher than the temperature of the system components, the components absorb heat from the environment, causing their temperatures to rise.

Figures 4E and 4F depict the influence of ambient temperature on the output power and efficiency of each module within the PV-TE-RC system. An increase in ambient temperature has a detrimental effect on the power and photovoltaic conversion efficiency of the photovoltaic module. As the ambient temperature increases from 0°C to 50°C, the power output of the PV module decreases from 88.01 W/m^2 to 82.06 W/m^2, and the photovoltaic conversion efficiency decreases from 10% to 9.32%. This decrease is a result of the rising ambient temperature, which reduces the heat dissipation from the PV module to the environment, leading to an increase in the module's temperature and, consequently, a decrease in both its photovoltaic conversion efficiency and power output. Conversely, the increase in ambient temperature has a positive impact on the cooling power, TEG power, and thermoelectric conversion efficiency. When the ambient temperature increases from 0°C to 50°C, the cooling power increases from −68 W/m^2 to 19.38 W/m^2, the TEG power increases from 0.13 W/m^2 to 0.98 W/m^2, and the thermoelectric conversion efficiency increases from 0.52% to 1.37%. Notably, when the ambient temperature surpasses 40°C, the cooling power changes from negative to positive. This signifies that higher ambient temperatures lead to increased cooling power, which is more conducive for the radiative cooling film to leverage its cooling capabilities. For the TEG module, the rise in ambient temperature enhances the energy density at both the hot and cold sides of the TEG, resulting in a greater temperature difference, which, in turn, increases power generation and thermoelectric conversion efficiency.

Solar intensity

Figure 5A illustrates the influence of solar irradiance on the temperatures of various points within the PV-TE-RC system. The temperatures of all measurement points are directly proportional to the solar irradiance. The most pronounced temperature change is observed for the PV module, which directly receives solar radiation, followed by the hot side and cold side of the TEG, and the radiative cooling film. This is

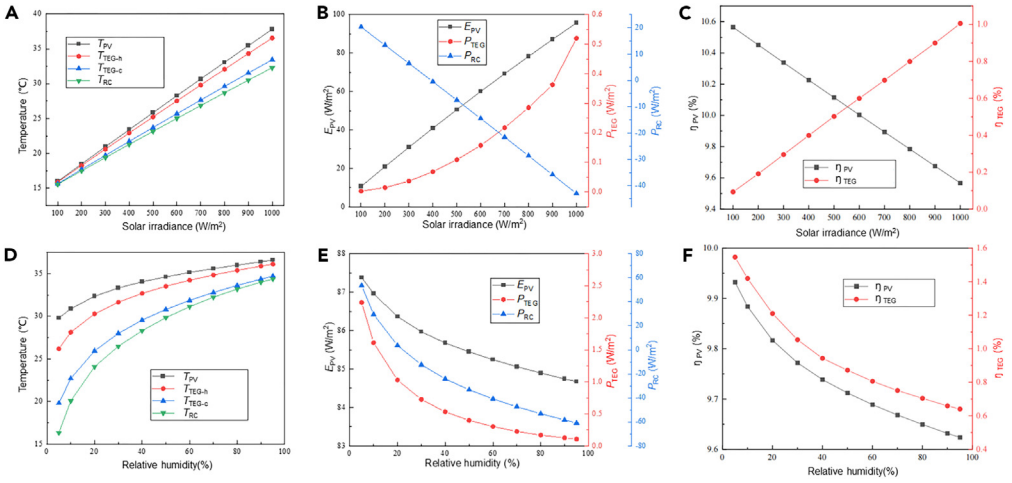

Figure 5. Effect of solar intensity (A–C) and relative humidity (D–F) on the thermal performance, output power, and conversion efficiency of the PV-TE-RC system

attributed to the fact that, with an increase in solar irradiance, the system components absorb more heat energy converted from solar irradiation, leading to a gradual temperature increase at each measurement point.

Figures 5B and 5C depict the effects of solar irradiance on the power output and efficiency of the PV-TE-RC system. An increase in solar irradiance positively impacts the power of the TEG and the PV module while exerting a negative influence on the cooling power. As solar irradiance escalates from 100 W/m^2 to 1000 W/m^2, the PV power surges from 10.57 W/m^2 to 95.67 W/m^2, the TEG power rises from 0.003 W/m^2 to 0.52 W/m^2, and the cooling power drops from 20.29 W/m^2 to −42.96 W/m^2. The heightened solar irradiance results in the PV cell absorbing more photon energy, leading to an increase in its power output. Additionally, the PV cell absorbs more energy beyond the bandgap, resulting in increased heating and transferring the excess heat to the hot side of the TEG through the thermal pipe. Consequently, the temperature differential between the cold and hot sides of the TEG widens, resulting in increased TEG power generation. For the radiative cooling module, when solar irradiance exceeds 350 W/m^2, the cooling power becomes negative, indicating that the heat input from solar irradiance surpasses the cooling produced. This occurs because the radiative cooling film receives direct sunlight, leading to an increase in heat input with rising solar irradiance, thereby reducing the cooling power. While the increase in solar irradiance negatively affects the photovoltaic conversion efficiency, it has a positive influence on the thermoelectric conversion efficiency. With irradiance varying from 100 W/m^2 to 1000 W/m^2, the photovoltaic conversion efficiency decreases from 10.57% to 9.57%, while the thermoelectric conversion efficiency increases from 0.09% to 1%. The heightened solar irradiance leads to increased absorption of solar energy by the PV cell, causing more energy from outside the bandgap to convert into heat, which raises its temperature, resulting in a deterioration of the output performance. Meanwhile, with the increase in solar irradiance, the heat flux density transferred to the TEG increases, elevating the temperature at the hot side of the TEG. Although the temperature on the cold side also rises, the temperature differential between the cold and hot sides of the TEG continues to increase, leading to an increase in thermoelectric conversion efficiency.

Relative humidity

Figure 5D illustrates the influence of relative humidity on the thermal performance of the PV-TE-RC system. As relative humidity increases, the temperatures of all system components gradually rise. When humidity exceeds 50%, the temperature at each point tends to level off. As humidity increases from 5% to 95%, the temperatures of the PV module, TEG hot side, TEG cold side, and radiative cooling membrane increase by 6.8°C, 9.94°C, 14.92°C, and 18.06°C, respectively. The increase in atmospheric water vapor content with higher humidity reduces the transmittance of the radiative cooling membrane in the "atmospheric window" range, which diminishes its ability to radiatively cool to outer space. Consequently, the cooling capacity provided by the radiative cooling membrane, serving as the cold source, decreases. This leads to an increase in the temperature of the radiative cooling membrane and, in turn, a decrease in the temperatures of other components.

Figures 5E and 5F demonstrate the effects of relative humidity on the output power and efficiency of the PV-TE-RC system. With humidity increasing from 5% to 95%, the PV power decreases from 87.38 W/m^2 to 84.68 W/m^2, and the photovoltaic conversion efficiency decreases from 9.93% to 9.62%. The TEG power decreases from 2.24 W/m^2 to 0.11 W/m^2, and the thermoelectric conversion efficiency decreases from 1.55% to 0.64%. The cooling power decreases from 53.6 W/m^2 to −60.9 W/m^2. The decrease in radiative cooling performance due to increased environmental humidity results in reduced radiative cooling power. As the temperature of the photovoltaic cells rises, their photovoltaic conversion efficiency decreases, leading to a reduction in photovoltaic power. Regarding the TEG, although the temperatures at both the hot and cold sides increase, the temperature difference between the two sides decreases, negatively affecting the TEG's power generation and thermoelectric conversion efficiency with increased humidity.

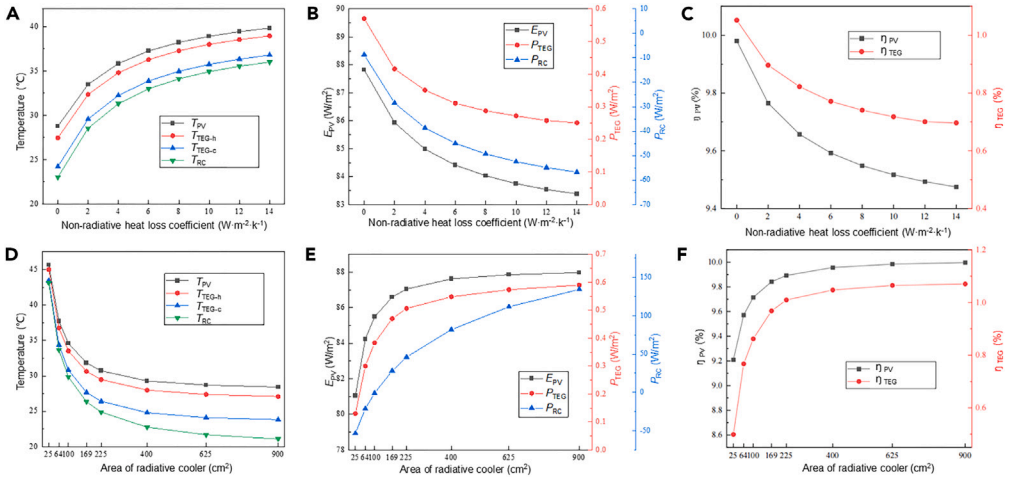

Figure 6. Effect of non-radiative heat loss coefficient (A–C) and area of radiative cooler (D–F) on the thermal performance, output power, and conversion efficiency of the PV-TE-RC system

Operating parameters

Non-radiative heat loss coefficient

Figure 6A illustrates the significant impact of the non-radiative heat loss coefficient on the radiative cooling performance of the film. As the non-radiative heat loss coefficient increases, the temperatures of all components gradually rise, with decreasing curve slopes. When the non-radiative heat loss coefficient increases from 0 W/(m^2·K) to 14 W/(m^2·K), the temperature of the PV module rises from 28.78°C to 39.84°C, the temperature of the hot side of the TEG increases from 27.46°C to 38.97°C, the temperature of the cold side of the TEG rises from 24.22°C to 36.8°C, and the temperature of the radiative cooling film climbs from 23.02°C to 36.02°C. The increase in the non-radiative heat loss coefficient results in greater cooling loss during the radiative cooling film's cooling process, causing the radiative cooling film's temperature to rise. This leads to elevated temperatures of the TEG cold and hot sides, as well as the PV module in thermal contact with it. Once the temperature of the radiative cooling film approaches the surrounding ambient temperature, the impact of further increasing the non-radiative heat loss coefficient on the temperatures of the system components weakens, and the increasing trend of each temperature point becomes smoother.

Figures 6B and 6C illustrate the impact of the non-radiative heat loss coefficient on the output power and efficiency of each module in the PV-TE-RC system. Increasing the non-radiative heat loss coefficient from 0 W/(m^2·K) to 14 W/(m^2·K) reduces the power of the PV cell from 87.82 W/m^2 to 83.38 W/m^2 and decreases its efficiency from 9.98% to 9.48%. Similarly, it reduces the TEG power from 0.57 W/m^2 to 0.25 W/m^2 and decreases its efficiency from 1.05% to 0.697%. The cooling power also decreases from −8.71 W/m^2 to −56.73 W/m^2. These results demonstrate that an increase in the non-radiative heat loss coefficient negatively impacts the thermal and electrical performance of the PV-TE-RC system. Reducing non-radiative heat loss is critical for improving the system's radiative cooling performance.

Area of radiative cooler

Figure 6D shows the influence of the area of the radiative cooler on the thermal performance of the PV-TE-RC system. Increasing the area of the radiative cooler results in lower temperatures for each component. However, as the area of the radiative cooler continues to increase, the declining trend in component temperatures becomes less prominent and tends to flatten. Specifically, as the area of the radiative cooler increases from 25 cm^2 to 900 cm^2, the temperature of the PV cell decreases from 45.64°C to 28.42°C, the temperature of the TEG's hot side decreases from 45°C to 27.09°C, the temperature of the TEG's cold side decreases from 43.42°C to 23.81°C, and the temperature of the radiative cooling film decreases from 43.11°C to 21.1°C.

Figures 6E and 6F illustrate the effects of the area of the radiative cooler on the output power and efficiency of each module in the PV-TE-RC system. As the area of the radiative cooler increases, the power output, efficiency, and cooling power of the PV cell, TEG, and thermoelectric conversion all gradually increase and then level off. When the area of the radiative cooler increases from 25 cm^2 to 900 cm^2, the power output of the PV cell increases from 81.05 W/m^2 to 87.97 W/m^2, the TEG power increases from 0.13 W/m^2 to 0.59 W/m^2, the cooling power increases from −53.36 W/m^2 to 134.23 W/m^2, the photoelectric conversion efficiency increases from 9.21% to 10%, and the thermoelectric conversion efficiency increases from 0.5% to 1.07%. The increase in the area of the radiative cooler provides more efficient energy exchange between the sky and outer space, resulting in greater cooling power and lower temperatures of the radiative cooling film. This, in turn, lowers the temperatures of the connected TEG and PV cell through heat conduction. The increased temperature difference between the cold and hot sides of the TEG improves the output performance of the PV cell and TEG. However, when the area of the radiative cooler exceeds 400 cm^2, the performance improvement of the system becomes less pronounced. This is due to the uneven distribution of temperature in the heat transfer area, with heat conduction being concentrated in the contact area between the TEG and the radiative cooler. As a result,

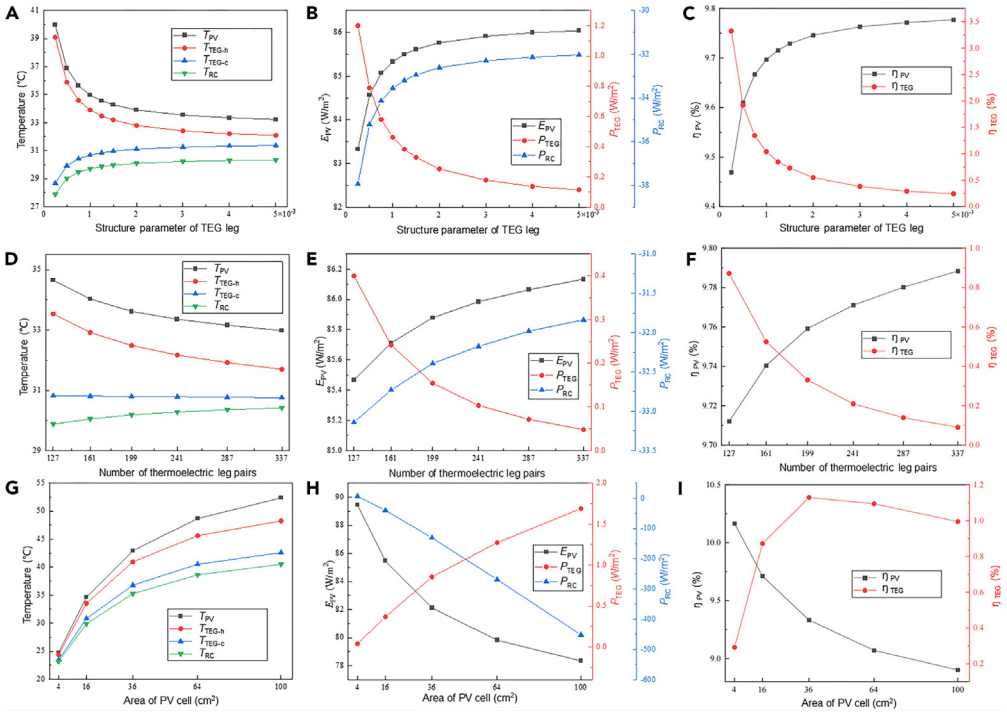

Figure 7. Effect of structure parameter of TEG leg (A–C), number of thermoelectric leg pairs (D–F), and area of PV cell (G–I) on the thermal performance, output power, and conversion efficiency of the PV-TE-RC system

the cooling energy provided by the enlarged area of the radiative cooler as the cold source input on the cold side of the TEG is not fully utilized. These results suggest that expanding the area of the radiative cooler can enhance the performance of the PV-TE-RC system, with the optimal area ratio of the radiative cooler to the TEG being 25.

Structure parameter of TEG leg

The structure parameter of the TEG leg refers to the ratio between the cross-sectional area and the height of the thermoelectric leg. The impact of changes in the structure parameter of the TEG leg on the thermoelectric performance of the PV-TE-RC system is depicted in Figure 7A. The structure parameter of the TEG leg exhibits a negative correlation with the temperature of the PV cell and the hot side of the TEG, while it demonstrates a positive correlation with the temperature of the cold side of the TEG and the radiative cooling film. The slopes of the temperature change curves for the four components gradually decrease as the structure parameter of the TEG leg increases. When the structure parameter of the TEG leg increases from 0.25×10^{-3} m to 5×10^{-3} m, the temperature of the PV cell decreases from 39.97°C to 33.23°C, the temperature of the hot side of the TEG decreases from 39.1°C to 32.09°C, the temperature of the cold side of the TEG increases from 28.68°C to 31.37°C, and the temperature of the radiative cooling film increases from 27.89°C to 30.34°C.

Figures 7B and 7C illustrate the influence of the structure parameter of the thermoelectric leg on the output power and efficiency of the PV-TE-RC system. Increasing the structure parameter of the TEG leg has a positive impact on the output performance and cooling power of the PV cell, while it exerts a negative effect on the TEG power generation and thermoelectric conversion efficiency. As the structure parameter of the TEG leg increases from 0.25×10^{-3} m to 5×10^{-3} m, the PV cell power increases from 83.33 W/m^2 to 86.04 W/m^2, the photovoltaic conversion efficiency rises from 9.47% to 9.78%, and the cooling power increases from −37.94 W/m^2 to −32 W/m^2. However, the TEG power and thermoelectric conversion efficiency decreased from 1.2 W/m^2 to 0.11 W/m^2 and from 3.32% to 0.24%, respectively. This phenomenon can be attributed to the increase in the structure parameter of the TEG leg, leading to a higher thermal conductivity within the TEG, favoring the internal heat transfer. With the heat flux density between the cold and hot sides of the TEG remaining constant, a smaller thermal resistance within the TEG results in a reduction in the temperature difference between the cold and hot sides. Consequently, the temperature at the hot side of the TEG decreases, while that at the cold side increases, thereby reducing the temperature difference and the TEG's electrical output performance. The TEG absorbs more waste heat generated by the PV cell, leading to a decrease in the PV cell temperature and an enhancement in its output performance. Due to the heat conduction among the system components, the radiative cooling film also exhibits an increase in temperature with the higher thermal conductivity of the TEG leg, resulting in a reduction in the loss of cold energy during the transfer between the TEGs. More cooling energy is transferred to the TEG and PV cell, leading to a gradual increase in the radiative cooling power. It is worth noting that the trends of the various parameters' increases or decreases become less pronounced as the structure parameter of the TEG leg further increases. This is because the radiative cooling film's transfer of cold energy to the cold side of the TEG is limited, as is the transfer

of heat from the PV cell to the hot side of the TEG. Consequently, as the structure parameter of the TEG leg increases, the two sides of the TEG, the cold side, and the hot side approach energy equilibrium, thereby maintaining the temperatures of the various components relatively stable. The optimal structure parameter of the TEG leg is 1.5.

Number of thermoelectric leg pairs

Figure 7D illustrates the influence of the number of thermoelectric leg pairs on the thermal performance of the PV-TE-RC system. As the number of thermoelectric leg pairs increases, both the PV cell temperature and the TEG hot-end temperature gradually decrease, with the slope of the curves decreasing. Meanwhile, the temperature of the radiative cooling film exhibits a small increase with the increase in the number of thermoelectric leg pairs, while the TEG cold-end temperature remains essentially unchanged. Specifically, as the number of thermoelectric leg pairs increases from 127 pairs to 337 pairs, the PV cell temperature decreases from 34.65°C to 32.98°C, and the TEG hot-end temperature decreases from 33.54°C to 31.7°C, while the temperature of the radiative cooling film increases from 29.88°C to 30.42°C.

The impacts of the number of thermoelectric leg pairs on the output power and efficiency of the PV-TE-RC system are illustrated in Figures 7E and 7F, respectively. From the figures, it is evident that an increase in the number of thermoelectric leg pairs has a positive effect on the PV cell power, the photovoltaic conversion efficiency, and the cooling power, while it hurts the TEG power generation and the thermoelectric conversion efficiency. As the number of thermoelectric leg pairs increases from 127 pairs to 337 pairs, the PV cell power increases from 85.47 W/m^2 to 86.13 W/m^2, the photovoltaic conversion efficiency increases from 9.71% to 9.79%, and the cooling power increases from −33.14 W/m^2 to −31.83 W/m^2. However, the TEG power decreases from 0.4 W/m^2 to 0.05 W/m^2, and the thermoelectric conversion efficiency decreases from 0.87% to 0.09%. Typically, a higher number of thermoelectric leg pairs in the TEG results in a higher Seebeck coefficient, which can generate greater output under the same temperature difference. However, the simulation results in this study yield a different conclusion, with the TEG's output power and photovoltaic conversion efficiency decreasing. This is because an increase in the number of thermoelectric leg pairs also implies a larger heat exchange area to facilitate the internal thermal exchange of the system components. Under the condition of a constant heat flow input and output at both sides, the temperature difference undoubtedly decreases, leading to a corresponding decrease in output power and thermoelectric conversion efficiency. Consequently, the temperature of the photovoltaic cell decreases, thereby improving the output performance of the photovoltaic module. Additionally, due to the thermal conduction between system components, the radiative cooling film exhibits an increase in temperature. The increase in the number of thermoelectric leg pairs reduces the thermal resistance of the TEG components, thereby reducing the heat transfer losses of the system. This consequently results in a gradual increase in radiative cooling power. However, with an increasing number of thermoelectric leg pairs, the improvements in the power generation and photovoltaic conversion efficiency of the photovoltaic cell and the radiative cooling power are not significant. The optimal number of thermoelectric leg pairs is 127 pairs.

Area of PV cell

Figure 7G illustrates the impact of the PV cell area on the performance of the PV-TE-RC system. Increasing the PV cell area results in varying degrees of temperature elevation for all components, with the most significant increase observed in the PV cell temperature, followed by the TEG hot side, TEG cold side, and the radiative cooling film. Specifically, as the PV cell area increases from 4 cm^2 to 100 cm^2, the PV cell temperature increases from 24.71°C to 52.38°C, the TEG hot side temperature increases from 24.35°C to 48.27°C, the TEG cold side temperature increases from 23.46°C to 42.61°C, and the radiative cooling film temperature increases from 23.14°C to 40.53°C.

Figures 7H and 7I illustrate the effects of the PV cell area on the output power and efficiency of the PV-TE-RC system. Increasing the PV cell area is beneficial for enhancing the power output of the PV cell, while there is a decreasing trend observed for the cooling power and photovoltaic conversion efficiency. Specifically, as the area of the PV cell increases from 4 cm^2 to 100 cm^2, the power output of the PV cell decreases from 89.46 W/m^2 to 78.34 W/m^2, the photovoltaic conversion efficiency decreases from 10.2% to 8.9%, and the cooling power decreases from 6.9 W/m^2 to −451.65 W/m^2. This phenomenon arises because a larger PV cell area implies more photons are converted into electrical energy. The PV cell absorbs more sunlight, leading to increased waste heat and elevated cell temperature, subsequently reducing the photovoltaic conversion efficiency. As the surplus heat generated by the PV module continues to increase, the cooling capacity provided by the radiative cooling module will no longer meet the system's cooling demands, leading to a decrease in the radiative cooling power to negative values. In contrast, as the area of the PV cell increases, the power output of the TEG gradually increases, while the thermoelectric conversion efficiency first increases and then decreases. When the area of the PV cell is small, increasing its area is beneficial for increasing the temperature difference between the cold and hot sides of the TEG, thereby improving the thermoelectric conversion efficiency. As the area of the PV cell further increases, the amount of heat transferred from the PV cell to the TEG significantly increases, while the effect of the cooling capacity provided by the radiative cooling film on the TEG temperature becomes minor. When the input heat on the TEG's hot side gradually increases, and the temperature difference between the two sides of the TEG does not increase significantly, the thermoelectric conversion efficiency will gradually decrease. The optimal PV cell area may depend on the specific goals and constraints of your PV-TE-RC system, but it's crucial to balance the trade-offs between PV cell power output, photovoltaic conversion efficiency, and cooling power to achieve the desired system performance.

DISCUSSION

The present study introduces a photovoltaic-thermoelectric-radiative cooling (PV-TE-RC) system that effectively harnesses both solar and space energy for high-quality, cooperative power generation. The system enables the comprehensive utilization of the full spectrum of two

thermodynamic resources and the hierarchical utilization of energy. To achieve this unique energy conversion mechanism, a stacked connection approach is adopted between the radiative cooling module and the thermoelectric module, while the thermoelectric module is indirectly connected to the photovoltaic cell module via thermal conductive pipes. The feasibility of the PV-TE-RC system's efficient operation throughout the day has been demonstrated. During the concentrated period of solar irradiation (11:00–13:00), the TEG generates an average power of 870 mW/m^2 by utilizing thermal energy and space energy, marking the highest value achieved to date for thermoelectric power generation based on radiative cooling. The ultra-high power generation performance is due to the harvesting of solar IR energy and PV thermochemical energy on the hot side of the TEG, while the cold side relies on the cooling provided by the radiative cooling film for heat dissipation, thus increasing the temperature difference between the hot and cold sides of the TEG. Additionally, the PV module provides supplementary electrical output from energies above the bandgap, leading to a power output of 85.87 mW/m^2, signifying a significant lead in power generation efficiency compared to all RC-TE systems. Therefore, the system maximizes the absorption of energy from both the sun and outer space for electricity generation, which is crucial for outdoor power generation. The design concept, methodology, and model of the reported PV-TE-RC system pave the way for the next generation of high-performance, highly adaptable, customizable, durable, cost-effective, and environmentally friendly passive power generation equipment, with extensive application prospects in the outdoor, military, and aerospace sectors.

Limitations of the study

We present a photovoltaic-thermoelectric-radiative cooling system that utilizes the full spectrum of sunlight and atmospheric window for power generation. However, the photovoltaic cells and TEG devices used in this study are commercial off-the-shelf products, which facilitate module integration but suffer from lower system output performance. Consideration may be given to adopting higher efficiency concentrator solar cells such as gallium arsenide or indium gallium arsenide, as well as thermoelectric materials with high ZT values, to enhance the thermal input of the system and maximize the utilization of temperature differentials, thereby improving system output performance.

STAR★METHODS

Detailed methods are provided in the online version of this paper and include the following:

- KEY RESOURCES TABLE
- RESOURCE AVAILABILITY
  - Lead contact
  - Materials availability
  - Data and code availability
- EXPERIMENTAL MODEL AND STUDY PARTICIPANT DETAILS
- METHOD DETAILS
  - Experimental process
  - System performance evaluation methods
  - Uncertainties
- QUANTIFICATION AND STATISTICAL ANALYSIS

SUPPLEMENTAL INFORMATION

Supplemental information can be found online at https://doi.org/10.1016/j.isci.2024.109952.

ACKNOWLEDGMENTS

This study was sponsored by the National Natural Science Foundation of China (NSFC52106268) and the National Natural Science Foundation of Hubei Province, China (No. 2022CFB748).

AUTHOR CONTRIBUTIONS

S.L. and Y.J. conceptualized the research and designed the research framework. H.B. conceived and designed the experiment. Y.L., J.Y., and Y.J. fabricated and assembled the PV-TE-RC system. R.J. and Y.J. conducted the outdoor test. Z.C., S.X., and Y.D. performed the calculations and analyzed the results. H.B. and S.L. wrote the paper. S.L. supervised the project. All authors read and commented on the manuscript.

DECLARATION OF INTERESTS

The authors declare no conflict of interest.

Received: December 19, 2023
Revised: April 29, 2024
Accepted: May 8, 2024
Published: May 9, 2024

REFERENCES

1. Gonzalez, J.M., Tomlinson, J.E., Martínez Ceseña, E.A., Basheer, M., Obuobie, E., Padi, P.T., Addo, S., Baisie, R., Etichia, M., Hurford, A., et al. (2023). Designing diversified renewable energy systems to balance multisector performance. Nat. Sustain. *6*, 415–427. https://doi.org/10.1038/s41893-022-01033-0.
2. Wang, S., Jiang, T., Meng, Y., Yang, R., Tan, G., and Long, Y. (2021). Scalable thermochromic smart windows with passive radiative cooling regulation. Science *374*, 1501–1504. https://doi.org/10.1126/science.abg0291.
3. Li, J., Wang, X., Liang, D., Xu, N., Zhu, B., Li, W., Yao, P., Jiang, Y., Min, X., Huang, Z., et al. (2022). A tandem radiative/evaporative cooler for weather-insensitive and high-performance daytime passive cooling. Sci. Adv. *8*, eabq0411. https://doi.org/10.1126/sciadv.abq0411.
4. Wang, X., Zhang, Q., Wang, S., Jin, C., Zhu, B., Su, Y., Dong, X., Liang, J., Lu, Z., Zhou, L., et al. (2022). Sub-ambient full-color passive radiative cooling under sunlight based on efficient quantum-dot photoluminescence. Sci. Bull. *67*, 1874–1881. https://doi.org/10.1016/j.scib.2022.08.028.
5. Zeng, S., Pian, S., Su, M., Wang, Z., Wu, M., Liu, X., Chen, M., Xiang, Y., Wu, J., Zhang, M., et al. (2021). Hierarchical-morphology metafabric for scalable passive daytime radiative cooling. Science *373*, 692–696. https://doi.org/10.1126/science.abi5484.
6. Zhou, L., Yin, X., and Gan, Q. (2023). Best practices for radiative cooling. Nat. Sustain. *6*, 1030–1032. https://doi.org/10.1038/s41893-023-01170-0.
7. Li, D., Liu, X., Li, W., Lin, Z., Zhu, B., Li, Z., Li, J., Li, B., Fan, S., Xie, J., and Zhu, J. (2021). Scalable and hierarchically designed polymer film as a selective thermal emitter for high-performance all-day radiative cooling. Nat. Nanotechnol. *16*, 153–158. https://doi.org/10.1038/s41565-020-00800-4.
8. Yin, X., Yang, R., Tan, G., and Fan, S. (2020). Terrestrial radiative cooling: Using the cold universe as a renewable and sustainable energy source. Science *370*, 786–791. https://doi.org/10.1126/science.abb0971.
9. Chen, Z., Zhu, L., Raman, A., and Fan, S. (2016). Radiative cooling to deep sub-freezing temperatures through a 24-h day-night cycle. Nat. Commun. *7*, 13729. https://doi.org/10.1038/ncomms13729.
10. Lu, X., Xu, P., Wang, H., Yang, T., and Hou, J. (2016). Cooling potential and applications prospects of passive radiative cooling in buildings: The current state-of-the-art. Renew. Sustain. Energy Rev. *65*, 1079–1097. https://doi.org/10.1016/j.rser.2016.07.058.
11. Essig, S., Allebé, C., Remo, T., Geisz, J.F., Steiner, M.A., Horowitz, K., Barraud, L., Ward, J.S., Schnabel, M., Descoeudres, A., et al. (2017). Raising the one-sun conversion efficiency of iii-v/si solar cells to 32.8% for two junctions and 35.9% for three junctions. Nat. Energy *2*, 17144. https://doi.org/10.1038/nenergy.2017.144.
12. Chen, C., Kuang, Y., and Hu, L. (2019). Challenges and opportunities for solar evaporation. Joule *3*, 683–718. https://doi.org/10.1016/j.joule.2018.12.023.
13. Yan, X., Lyu, S., Xu, X.-Q., Chen, W., Shang, P., Yang, Z., Zhang, G., Chen, W., Wang, Y., and Chen, L. (2022). Superhydrophilic 2d covalent organic frameworks as broadband absorbers for efficient solar steam generation. Angew. Chem. Int. Ed. Engl. *61*, e202201900. https://doi.org/10.1002/anie.202201900.
14. Wang, X., Liu, Q., Wu, S., Xu, B., and Xu, H. (2019). Multilayer polypyrrole nanosheets with self-organized surface structures for flexible and efficient solar-thermal energy conversion. Adv. Mater. *31*, 1807716. https://doi.org/10.1002/adma.201807716.
15. Wu, Z., Zhang, S., Liu, Z., Mu, E., and Hu, Z. (2022). Thermoelectric converter: Strategies from materials to device application. Nano Energy *91*, 106692. https://doi.org/10.1016/j.nanoen.2021.106692.
16. Jurado, J.P., Dörling, B., Zapata-Arteaga, O., Roig, A., Mihi, A., and Campoy-Quiles, M. (2019). Solar harvesting: A unique opportunity for organic thermoelectrics? Adv. Energy Mater. *9*, 1902385. https://doi.org/10.1002/aenm.201902385.
17. Kraemer, D., Jie, Q., McEnaney, K., Cao, F., Liu, W., Weinstein, L.A., Loomis, J., Ren, Z., and Chen, G. (2016). Concentrating solar thermoelectric generators with a peak efficiency of 7.4. Nat. Energy *1*, 16153. https://doi.org/10.1038/nenergy.2016.153.
18. Li, K., Sun, X., Wang, Y., Wang, J., Dai, X., Li, G., and Wang, H. (2022). All-in-one single-piece flexible solar thermoelectric generator with scissored heat rectifying p-n modules. Nano Energy *93*, 106789. https://doi.org/10.1016/j.nanoen.2021.106789.
19. Min, X., Wang, X., Li, J., Xu, N., Du, X., Zeng, M., Li, W., Zhu, B., and Zhu, J. (2023). A smart thermal-gated bilayer membrane for temperature-adaptive radiative cooling and solar heating. Sci. Bull. *68*, 2054–2062. https://doi.org/10.1016/j.scib.2023.08.003.
20. Zhang, S., Wu, Z., Liu, Z., and Hu, Z. (2023). An emerging energy technology: Self-uninterrupted electricity power harvesting from the sun and cold space. Adv. Energy Mater. *13*, 2300260. https://doi.org/10.1002/aenm.202300260.
21. Raman, A.P., Anoma, M.A., Zhu, L., Rephaeli, E., and Fan, S. (2014). Passive radiative cooling below ambient air temperature under direct sunlight. Nature *515*, 540–544. https://doi.org/10.1038/nature13883.
22. Liu, J., Zhang, J., Tang, H., Zhou, Z., Zhang, D., Ye, L., and Zhao, D. (2021). Recent advances in the development of radiative sky cooling inspired from solar thermal harvesting. Nano Energy *81*, 105611. https://doi.org/10.1016/j.nanoen.2020.105611.
23. Chen, Z., Zhu, L., Li, W., and Fan, S. (2019). Simultaneously and synergistically harvest energy from the sun and outer space. Joule *3*, 101–110. https://doi.org/10.1016/j.joule.2018.10.009.
24. Zhan, Z., ElKabbash, M., Li, Z., Li, X., Zhang, J., Rutledge, J., Singh, S., and Guo, C. (2019). Enhancing thermoelectric output power via radiative cooling with nanoporous alumina. Nano Energy *65*, 104060. https://doi.org/10.1016/j.nanoen.2019.104060.
25. Ren, W., Sun, Y., Zhao, D., Aili, A., Zhang, S., Shi, C., Zhang, J., Geng, H., Zhang, J., Zhang, L., et al. (2021). High-performance wearable thermoelectric generator with self-healing, recycling, and lego-like reconfiguring capabilities. Sci. Adv. *7*, eabe0586. https://doi.org/10.1126/sciadv.abe0586.
26. Liu, Y., Hou, S., Wang, X., Yin, L., Wu, Z., Wang, X., Mao, J., Sui, J., Liu, X., Zhang, Q., et al. (2022). Passive radiative cooling enables improved performance in wearable thermoelectric generators. Small *18*, 2106875. https://doi.org/10.1002/smll.202106875.
27. Jung, Y., Jeong, S., Ahn, J., Lee, J., and Ko, S.H. (2023). High efficiency breathable thermoelectric skin using multimode radiative cooling/solar heating assisted large thermal gradient. Small *20*, 2304338. https://doi.org/10.1002/smll.202304338.
28. Mu, E., Wu, Z., Wu, Z., Chen, X., Liu, Y., Fu, X., and Hu, Z. (2019). A novel self-powering ultrathin teg device based on micro/nano emitter for radiative cooling. Nano Energy *55*, 494–500. https://doi.org/10.1016/j.nanoen.2018.10.057.
29. Raman, A.P., Li, W., and Fan, S. (2019). Generating light from darkness. Joule *3*, 2679–2686. https://doi.org/10.1016/j.joule.2019.08.009.
30. Liao, M., Banerjee, D., Hallberg, T., Åkerlind, C., Alam, M.M., Zhang, Q., Kariis, H., Zhao, D., and Jonsson, M.P. (2023). Cellulose-based radiative cooling and solar heating powers ionic thermoelectrics. Adv. Sci. *10*, e2206510. https://doi.org/10.1002/advs.202206510.
31. Khan, S., Kim, J., Roh, K., Park, G., and Kim, W. (2021). High power density of radiative-cooled compact thermoelectric generator based on body heat harvesting. Nano Energy *87*, 106180. https://doi.org/10.1016/j.nanoen.2021.106180.
32. Omair, Z., Assawaworrarit, S., Fan, L., Jin, W., and Fan, S. (2022). Radiative-cooling-based nighttime electricity generation with power density exceeding 100 mw/m2. iScience *25*, 104858. https://doi.org/10.1016/j.isci.2022.104858.
33. Chen, C., Zhao, B., Wang, R., He, Z., Wang, J.L., Hu, M., Li, X.L., Pei, G., Liu, J.W., and Yu, S.H. (2022). Janus helical ribbon structure of ordered nanowire films for flexible solar thermoelectric devices. Adv. Mater. *34*, 2206364. https://doi.org/10.1002/adma.202206364.
34. Han, W.B., Heo, S.Y., Kim, D., Yang, S.M., Ko, G.J., Lee, G.J., Kim, D.J., Rajaram, K., Lee, J.H., Shin, J.W., et al. (2023). Zebra-inspired stretchable, biodegradable radiation modulator for all-day sustainable energy harvesters. Sci. Adv. *9*, eadf5883. https://doi.org/10.1126/sciadv.adf5883.
35. Guo, J., and Huai, X. (2023). Maximizing electric power through spectral-splitting photovoltaic-thermoelectric hybrid system integrated with radiative cooling. Adv. Sci. *10*, 2206575. https://doi.org/10.1002/advs.202206575.
36. Kim, S., Park, J.H., Lee, J.W., Kim, Y., and Kang, Y.T. (2023). Self-recovering passive cooling utilizing endothermic reaction of nh4no3/h2o driven by water sorption for photovoltaic cell. Nat. Commun. *14*, 2374. https://doi.org/10.1038/s41467-023-38081-9.
37. Price, M.B., Butkus, J., Jellicoe, T.C., Sadhanala, A., Briane, A., Halpert, J.E., Broch, K., Hodgkiss, J.M., Friend, R.H., and Deschler, F. (2015). Hot-carrier cooling and photoinduced refractive index changes in organic-inorganic lead halide perovskites. Nat. Commun. *6*, 8420. https://doi.org/10.1038/ncomms9420.
38. Li, M., Fu, J., Xu, Q., and Sum, T.C. (2019). Slow hot-carrier cooling in halide perovskites: Prospects for hot-carrier solar cells. Adv. Mater. *31*, 1802486. https://doi.org/10.1002/adma.201802486.

39. Lv, S., Zhang, B., Ji, Y., Ren, J., Yang, J., Lai, Y., and Chang, Z. (2023). Comprehensive research on a high performance solar and radiative cooling driving thermoelectric generator system with concentration for passive power generation. Energy *275*, 127390. https://doi.org/10.1016/j.energy.2023.127390.

40. Bahaidarah, H., Subhan, A., Gandhidasan, P., and Rehman, S. (2013). Performance evaluation of a pv (photovoltaic) module by back surface water cooling for hot climatic conditions. Energy *59*, 445–453.

41. Yousef, M.S., Abdel Rahman, A.K., and Ookawara, S. (2016). Performance investigation of low - concentration photovoltaic systems under hot and arid conditions: Experimental and numerical results. Energy Convers. Manag. *128*, 82–94. https://doi.org/10.1016/j.enconman.2016.09.061.

42. Liao, T., He, Q., Xu, Q., Dai, Y., Cheng, C., and Ni, M. (2021). Coupling properties and parametric optimization of a photovoltaic panel driven thermoelectric refrigerators system. Energy *220*, 119798. https://doi.org/10.1016/j.energy.2021.119798.

43. Moffat, R.J. (1988). Describing the uncertainties in experimental results. Exp. Therm. Fluid Sci. *1*, 3–17. https://doi.org/10.1016/0894-1777(88)90043-X.

STAR★METHODS

KEY RESOURCES TABLE

REAGENT or RESOURCE	SOURCE	IDENTIFIER
Software and algorithms		
COMSOL Multiphysics 5.6	COMSOL Co., Ltd.	https://cn.comsol.com/
MATLAB 2019a	Mathworks	https://www.mathworks.com/products/matlab.html
Other		
TEG device	Hubei Sagreon New Energy Technology Company, Ltd.	http://www.hbsagreon.com/cgwcfdxp/article-4.html
Heat pipe	Xuzhou Reer Electronic Technology Co., Ltd.	YT60-120
Monocrystalline silicon solar cells	Anyang City Sunshine Science and Education Energy Co., Ltd.	http://www.aykjw.com/Product-detail-id-539813.html
Solar module analyzer	Taiwan PROVA	PROVA-210
Portable data logger	HIOKI, Japan	https://www.hioki.cn/products/102.html

RESOURCE AVAILABILITY

Lead contact

Requests for further information and resources should be directed to the lead contact, Lv Song (lvsong@whut.edu.cn).

Materials availability

This study did not generate new unique reagents.

Data and code availability

- All data can be obtained from the lead contact, provided the request is reasonable.
- The code related to the developed model can be accessed by reaching out to the lead contact.
- Any additional information required to reanalyze the data reported in this paper is available from the lead contact upon request.

EXPERIMENTAL MODEL AND STUDY PARTICIPANT DETAILS

The models in this research are based on classical energy balance equations.

METHOD DETAILS

Experimental process

According to the provided description, the experimental setup of the PV-TE-RC system includes a transparent cover plate and a radiative cooling film. The transparent cover plate is made of low-density polyethylene film with a thickness of 0.5 μm, exhibiting high light transmission performance. Its primary function is to reduce the heat exchange between the radiative cooling module and the environment caused by air convection. The radiative cooling film is composed of a TiO_2/PMMA composite film, positioned in the center of the device with dimensions of 100 mm × 100 mm × 0.4 mm. Polystyrene extruded boards are arranged around the four sides and the bottom of the radiative cooling film to minimize cooling loss and provide support for the device. The outer surface of the extruded boards is wrapped with aluminum foil to reduce the heat absorbed by the radiative cooling device due to solar irradiation. The distance between the radiative cooling film and the transparent cover plate is 10 mm, forming a cooling space enclosed by them. The preparation process of each component in the system and the characterization methods can be found in the supporting materials.

System performance evaluation methods

For the photovoltaic cell module, the photoelectric conversion efficiency is an important index for evaluating its performance, which is usually used to measure the ability to convert solar radiation energy into electrical energy. The expression for instantaneous photoelectric conversion efficiency be written as[41]:

$$\eta_{PV} = \frac{E_{PV}}{A_{PV} G}$$

where, G is the solar radiation intensity, W/m^2.

For thermoelectric modules, the thermoelectric conversion efficiency is an important parameter used to evaluate the performance of thermoelectric materials, which refers to the ability of a thermoelectric device to convert thermal energy into electrical energy. It can be written as follows[42]:

$$\eta_{teg} = \frac{P_{TEG}}{E_{TEG-h} \cdot A_{TEG}}$$

where, $E_{TEG\text{-}h}$ is the heat flow density, W/m^2, A_{TEG} is the area of the thermoelectric device, m^2.

For a no-load circuit, the output power of the thermoelectric device can be determined from the open circuit voltage U and the internal resistance r. The equation can be written as[28]:

$$P_{TEG} = \frac{U^2}{r}$$

where, r is the internal resistance of the TEG, Ω; U is the open-circuit voltage of the TEG, V, it can be calculated by the following formula[28]:

$$U = n \cdot S \cdot (T_h - T_a)$$

The optimum efficiency of a thermoelectric device refers to the highest efficiency under a given temperature difference. To achieve the optimal efficiency of a thermoelectric device, factors such as thermoelectric materials, structural optimization, and temperature differences need to be considered. By optimizing the thermoelectric device, the optimal efficiency is written as[42]:

$$\eta_{TEG} = \frac{T_{TEG-h} - T_{TEG-c}}{T_{TEG-h}} \cdot \frac{\sqrt{1+ZT} - 1}{\sqrt{1+ZT} + \frac{T_{TEG-h}}{T_{TEG-c}}}$$

For the PV-TE-RC system, the total efficiency is an essential index for evaluating the system performance and is usually used to measure the ability of the system to convert solar radiant energy into electrical energy, which can be written as:

$$\eta_{PV-TE-RC} = \frac{E_{pv} + P_{TEG}}{A_{pv} G}$$

Uncertainties

The uncertainty analysis is performed using the square root of the sum of the squared errors from each error source as proposed by Moffat.[43] The uncertainties of each module temperature mainly stem from the accuracy of the thermocouple (±3.7%) and the calibration uncertainty (±7.0%). Solar irradiance uncertainties primarily arise from repeatability (±8.0%) and measurement error (±3.0%). The uncertainties of PV efficiency are mainly from the accuracy of the solar module analyzer (±1.0%) and repeatability measurement error (±5.0%). TEG efficiency uncertainties originate from the electric energy meter (±2.0%) and repeatability measurement error (±5.0%). Consequently, the final uncertainties for temperature, solar irradiance, PV efficiency, and TEG efficiency are ±7.9%, ±8.5%, ±5.1%, and ±5.4%, respectively.

QUANTIFICATION AND STATISTICAL ANALYSIS

Statistical analysis of data was performed using Excel (Microsoft) and Origin (OriginLab).